Cumhuriyet Sci. J., 44(2) (2023) 302-314
DOI: https://doi.org/10.17776/csj.1258573

Cumhuriyet Science Journal

| csj.cumhuriyet.edu.tr | Founded: 2002 ISSN: 2587-2680 e-ISSN: 2587-246X Publisher: Sivas Cumhuriyet University

Design, Characterization and in vitro Simulations of nano-HAP/GO Composite Drug Delivery System Produced by Hydrothermal Methods Loaded with Paclitaxel

Fatih Çiftçi [1,2,a,*]

[1] *Department of Biomedical Engineering, Fatih Sultan Mehmet Vakif University, İstanbul, Türkiye.*
[2] *Department of Technology Transfer Office, Fatih Sultan Mehmet Vakif University, İstanbul, Türkiye*
**Corresponding author*

Research Article

History
Received: 01/03/2023
Accepted: 19/06/2023

ABSTRACT

In this study, it was aimed to develop a nano drug system that can be used in passive targeting in pancreatic cancer treatment. Hydroxyapatite nanocrystals (n-HAP) produced by hydrothermal process and graphene oxide (GO) produced by hummers method were used to increase the carrier capacity of the nano drug system and to activate the drug release kinetics and drug loading capacity. Analyses performed for nanocomposite drug carrier systems; FT-IR, XRD, TGA, BET analysis, Zeta potential, TEM and SEM. Paclitaxel (PTX), a chemotherapeutic drug used in the treatment of pancreatic cancer, was loaded into HAP nanocrystals (PTX- loaded n-HAP) and its activity on pancreatic cancer cells was investigated. When PTX was 1 and 2 mg, Encapsulation Efficiency (EE) and Drug Loading Content (LC) were 79.17-72.24% and 80.01-80.27%, respectively, for H-n-HAP crystal structure only, while EE and LC were 88.57-81.57% and 90.84-110.57%, respectively, when H-n-HAP crystal structure was loaded with 1 and 2 mg PTX together with GO. Here, it was observed PTX release profiles are according to the Hixson model. According to Fick's law, release profile was observed with values of k=1.89, n=0.21, SSD=0.04, R^2=0.997, FIC=2.03, SD=0.004. In cell culture studies, as GO nanomaterials were loaded into H-n-HAP nanocrystal structure, the effect of PTX drug on pancreatic cancer increased and the viability of cancer cells decreased. It can be concluded that H-n-HAP/GO/PTX nanocomposite structure kills more pancreatic cancer cells with synergistic effect.

Keywords: Biodegradable material, Graphene, Nano-structures, Nanocomposite, Biopolymer.

[a] *faciftcii@gmail.com* *https://orcid.org/0000-0002-3062-2404*

Introduction

The main objectives in designing nanoparticles as drug delivery systems include controlling particle size, surface properties and release of pharmacologically active substances to ensure targeted site-specific delivery of the drug at therapeutically optimal rate and dose [1]. Nanoparticle-based drugs control and sustain the release of the drug during transport and at the site of localization, as well as enabling the distribution of the drug to organs and subsequent clearance of the drug to increase the therapeutic efficacy of the drug and reduce its side effects [2], [3]. The controlled release and particle degradation properties of nanoparticles can be easily modulated by the choice of matrix components. The drug loading of nanoparticles is relatively high and drugs can be incorporated into the systems without any chemical reaction, an important factor for maintaining drug activity. Site-specific targeting can be achieved by binding target ligands to the surface of the particles or by using magnetic guidance. Drug delivery systems created with nanoparticles can be used in various routes of administration, including oral, nasal, parenteral, intraocular [4], [5].

Many methods have been developed to produce nano-sized hydroxyapatite (n-HAP) crystals [6]. The most commonly used methods include sol-gel method, micro-emulsion method, hydrothermal method and wet chemical method. Among these, the hydrothermal method is the most widely used method because it is easy in terms of applicability. However, many studies have shown that the technique of nano-sized hydroxyapatite (H-n-HAP) synthesis by hydrothermal method can be improved with drug release enhancing surfactant additives [7]–[10].

Changing some parameters (temperature, time, pH value) during the hydroxyapatite (HAP) production process affects the solubility and crystallinity of the produced structure. HAP is used in many fields, especially in drug delivery systems and tissue engineering. Much of the 3D manufacturing of ceramics in biomedicine is for the creation of pure ceramic scaffolds that mimic the minerals, structures and mechanical properties naturally found in bone. In addition, powdered HAP is also widely used in 3D fabrication, thanks to its presence as a calcium phosphate phase in mineralized bone.

The other material to be used in this study is graphene oxide (GO), a surfactant and bioactive agent with drug release kinetics enhancing properties. GO, which will be used together with HAP in this study, is a highly oxidized

chemically modified graphene consisting of a one-atom thick layer of graphene sheets with carboxylic acid, epoxide and hydroxyl groups in the plane. GO, which is a carbon nanomaterial, acts as a bridge to cells and increases cell adhesion because it has more surface functional groups [11]. The basal plane also contains free surface π electrons from unmodified domains of graphene with π-π interaction capabilities for hydrophobic and non-covalent functionality. Thus, GO is an amphiphilic sheet-like molecule that can be used as a surfactant to stabilize hydrophobic molecules in a solution [12]. GO has low cytotoxicity and antibacterial properties. The large surface area volume and biocompatibility of GO, which has high mechanical properties and high corrosion resistance, increase its use in nanocomposite applications [12], [13]. GO's mechanical properties tolerate stress, thus improving interface bonding and chemical adhesion [14]. Furthermore, GO nanosheets have been used as a material with large surface area in drug delivery applications by increasing their loading capacity [15]. As an innovative application on this subject; in vitro cell viability tests were performed on GO and HAP and it was reported that antibacterial studies of these nanocomposites, which exhibited high cell viability, completely inhibited *E. coli* growth [16].

Localized or targeted delivery of chemotherapeutics has been used in recent trends to limit indiscriminate toxicities to normal tissues associated with chemotherapy. Paclitaxel (PTX), the first of a new class of microtubule-stabilizing agents, is recognized as an effective chemotherapeutic agent for a wide range of solid tumors. The clinical application of this highly effective drug in cancer therapy is limited due to its poor aqueous solubility and poor oral bioavailability. To date, only two commercial formulations have been developed. The first formulation developed uses a 1:1 mixture of CremophorEL and ethanol to improve the solubility of intravenously administered paclitaxel. CremophorEL has been shown to have serious side effects including severe hypersensitivity reactions, neurotoxicity and hypotensive vasodilation. The most recent development in PTX administration is that an injectable suspension of albumin bound PTX nanoparticles called Abraxane has shown effective results. However, not only is bone marrow suppression a dose-dependent and dose-limiting toxicity but neuropathy toxicity has also been shown to be remarkably increased compared to the conventional PTX formulation. Therefore, safe and effective drug delivery systems are needed to improve the safety and therapeutic efficacy of current clinical chemotherapeutic treatments.

This study aims to develop a model to enhance the release kinetics activity of paclitaxel (PTX) in pancreatic cancer by doping surface-activating graphene oxides (GOs) into nano-sized hydroxyapatites (n-HAP) produced using the hydrothermal method. The objective is to investigate and determine whether chemotherapeutic drugs used in cancer treatment, along with active agents, can exhibit increased shelf-life effects. The feasibility of a proposed approach using PTX as the model drug for controlled drug delivery devices is explored. The study focuses on searching for the optimal differences in Quantitative Structure-Property Relationship (QSPR) models for mutual diffusion, as well as predictive QSPR models for release kinetics based on the Hixson mathematical model.

Materials and Methods

Production of Hydroxyapatite Crystals by Hydrothermal Method

The chemicals used were calcium nitrate tetrahydrate ($Ca(NO_3)_2.4H_2O$; Merck KGaA, Darmstadt, Germany) and di-ammonium hydrogen phosphate ($(NH_4)2HPO_4$; Merck, KGaA, Darmstadt, Germany). The amount of starting materials for Hydroxyapatite (HAP) synthesis was determined as Ca/P ratio of 1.67. 23.66 g of $Ca(NO_3)_2.4H_2O$ was dissolved in 100 ml of water. The prepared $Ca(NO_3)_2.4H_2O$ and $(NH_4)2HPO_4$ were mixed in an ultrasonic bath for 15 minutes. A stock solution was prepared by dissolving 7.93 g of $(NH_4)2HPO_4$ in 100 ml of water. The pH of the prepared solutions was adjusted to pH≥10 with a drop of ammonia solution (NH_4OH, 28%, Merck Co. Darmstadt, Germany) to bring the pH ≥10. Prepared $Ca(NO_3)_2.4H_2O$ and $(NH_4)2HPO_4$ stock solutions were taken 20 ml each and mixed dropwise. The resulting nano-sized hydroxyapatite (n-HAP) crystals were kept at room temperature for 24 hours to precipitate. It was washed 6 times at 4100 rpm for 5 minutes to remove the residues formed as a result of the reaction. As in the wet chemical method, the n-HAPs produced were placed in the cell in the hydrothermal reactor after waiting for 24 hours for precipitation. n-HAPs were poured into the cell of the hydrothermal reactor, placed in the hydrothermal reactor and tightly closed. The n-HAPs placed in the hydrothermal reactor were allowed to react at 200 °C for 2 hours. After the reaction, the hydrothermal reactor was allowed to cool down and the hydroxyapatites formed were carefully removed from the reactor. The hydroxyapatites were washed 6 times at 4100 rpm for 5 minutes to remove the residues formed as a result of the reaction.

PTX Albumin-stabilized Nanoparticle Formulation Hydrothermal Treatment of Nano-Sized Hydroxyapatite Crystals

A 1mg/ml PTX solution was prepared by dissolving 50 mg lyophilized PTX in 50 ml water for injection. Stock $Ca(NO3)_2{\cdot}4H_2O$ solution and stock $(NH_4)H_2PO_4$ solution were taken 20 ml each. The pH of these solutions was adjusted to ≥10 with ammonia. The prepared 1mg/ml PTX solution was added dropwise to the $Ca(NO3)_2{\cdot}4H_2O$ solution. The pH was checked again and if it was lower than 10, it was adjusted again by adding ammonia to ≥10. The resulting $Ca(NO3)_2{\cdot}4H_2O$-PTX solution was mixed dropwise into $(NH_4)H_2PO_4$ solution. The resulting PTX-loaded nanostructured n-HAP crystals were kept at room temperature for 24 hours to precipitate. After 24 hours at

room temperature, half of the PTX-loaded n-HAP crystals were separated and with washed pure water 10 times at 4100 rpm for 5 min to remove by-products and residues. After precipitation of PTX-loaded n-HAP crystals formed by wet chemical method, the separated half was poured into the cell inside the hydrothermal reactor. After placing the cell in the hydrothermal reactor, the reactor was closed tightly. The PTX-loaded n-HAPs in the reactor were allowed to react at 200°C for 2 hours. After the reaction took place, the hydrothermal reactor was allowed to cool down. After the reactor cooled down, the PTX-loaded n-HAP crystals in the reactor were washed 10 times at 4100 rpm for 5 min to remove by-products and residues. All samples obtained were frozen at -20 °C to prepare for the lyophilizer. n-HAP crystals, hydrothermal n-HAP crystals, PTX-loaded n-HAP crystals and hydrothermal PTX-loaded n-HAP crystals were placed in the lyophilizer for 24 hours.

GO Loading and Preparation of Ptx/N-Hap Nanostructures

In this study, GO was synthesized by Hummers' method [17]. The chemicals used for synthesis such as Graphite flake (mesh size 300), Sulfuric acid (H_2SO_4) potassium permanganate ($KMnO_4$, 99.9%), phosphoric acid (H_3PO_4) and hydrogen peroxide (H_2O_2 30%) were purchased from Merck and Sigma Aldrich. These 1% GO ratio solutions were prepared as the each given amount (ml) in 10 ml distilled water and 10 min. ultra-sonication were applied. These amounts were calculated to produce 1 g nanocomposite product. 2.35 g $Ca(NO3)_2{\cdot}4H_2O$ was added to each GO solutions pH adjusted ≥10 with ammonium. In the continuation 2,37 g $(NH_4)H_2PO_4$ were dissolved in 10 ml distilled water and pH adjusted ≥10 with ammonium for each 3 beakers for 1% GO ratio.

The hydrothermal system was loaded after different experimental runs to n-HAP of the two materials. First n-HAP production, then hydrothermal production by loading PTX into n-HAP, and finally hydrothermal method was realised by loading GO nanomaterial separately PTX/n-HAP and n-HAP. In this study, the working groups were separated as PTX/n-HAP/GO and n-HAP and the hydrothermal method was carried out after the wet chemistry method.

Characterizations

Particle Size, Size Distribution and Zeta Potential

The average particle size, polydispersity index and zeta potential of hydrothermal n-HAP crystals, hydrothermal n-HAP/GO nanocomposites, PTX-loaded n-HA crystals, hydrothermal PTX-loaded n-HAP/GO nanostructures were measured by photon correlation spectroscopy using Zetasizer (Nano ZS, Malvern, UK) with DLS method. Measurements were performed three times for each sample at a 90° angle and the samples were kept at 25 °C. Each sample was diluted with deionized water before measurement. The zeta potentials of the prepared nanoparticles were determined with an electric field electrophoretic cell using the same equipment.

Fourier-Transform Infrared Spectroscopy Analysis

GO functional groups and PTX chemical bonds and functional groups of hydrothermal n-HAP crystals, hydrothermal n-HAP/GO nanocomposites, PTX-loaded n-HA crystals, hydrothermal PTX-loaded n-HAP/GO nanostructures, GO functional groups and PTX chemical bonds and functional groups were determined by Fourier Transform Infrared Spectrophotometer (Alpha FTIR Spectroscopy, Bruker, USA) at wavelength 4000-750 cm^{-1}.

Scanning Electron Microscopy and EDS Mapping & Spotting

The morphological analysis of the nanocomposite structures was observed by scanning electron microscopy (SEM) (EVO LS 10, ZEISS). The operating conditions were 5 kV and secondary backscattered electrons mode. The imageable parts were examined with a voltage of 10 kV. All samples were coated with gold-palladium to ensure conductivity as the nanostructures lack this property. Morphological features, elemental analysis and homogeneity of the samples were analyzed by EDX (Energy Dispersive X-Ray Spectrometry). EDAX Element 2016 was used for EDS mapping and staining analysis. Elemental differences and homogeneity between two spots were investigated. Spots that appear different from each other were compared. Pore sizes were also measured. Staining was achieved by SEM with a Cathodoluminescence Detector (CL) attached. In some cases, the BSD-Back Scatter Detector was used to look for differences between elements. EDS spots (1-2-3) were showed in Figure 5.A as red, green and blue respectively.

Brunauer-Emmett-Teller Analysis

Hydrothermal n-HAP crystals, hydrothermal n-HAP/GO nanocomposites, PTX-loaded n-HA crystals, hydrothermal PTX-loaded n-HAP/GO nanostructures, PTX powders and GO carbon nanostructures were used to obtain information about the surface areas. The suspensions were prepared using a 1% sample concentration. To measure the surface area, standard BET (Brunauer-Emmett-Teller; Micromeritics TriStar II) degassing conditions were applied. The powders were heated for 1 hour at 90°C followed by 2 hours at 250°C to eliminate any organic substances present in both the synthetic water and the synthesized powders. This process ensured that the surface area measurements were accurate by removing any potential interference from organic compounds.

X-ray Diffraction Analysis

X-ray Diffraction (XRD; Braket XPERT-PRO; measurement with Cu (Copper) internal wavelengths anode) was used to determine the phase structures of hydrothermal n-HAP crystals, hydrothermal n-HAP/GO nanocomposites, PTX-loaded n-HA crystals, hydrothermal PTX-loaded n-HAP/GO nanostructures, PTX powders and GO carbon nanostructures. It was investigated patterns between 10 to 70^o angle by using 40 mA and 45 kV generator.

Thermogravimetric Analysis (TG-DTA)

The thermal behaviour of hydrothermal n-HAP crystals, hydrothermal n-HAP/GO nanocomposites, PTX-loaded n-HA crystals, hydrothermal PTX-loaded n-HAP/GO nanostructures, PTX powders and GO carbon nanostructures were studied by differential thermal analysis (DTA) and thermal gravimetric analysis (TGA) using an SDT Q600 analyser at 25- 900℃. The analyses were performed in dry air.

HPLC method

Percent nanoparticle yield was calculated as the ratio of the total weight of lyophilized nanoparticle powder obtained to the total weight of all formulation components used multiplied by 100. Percent PTX loading was calculated by multiplying 100 by the ratio of the total amount of drug extracted from the polymeric matrix with a known nanoparticle weight to the total weight of nanoparticles used prior to extraction. The encapsulation efficiency was calculated by multiplying 100 by the ratio of the weight of the drug contained in a nanoparticle batch to the weight of the drug used in the formulation (the actual amount). Briefly, approximately 10 mg of correctly weighted lyophilized nanoparticles were dispersed in an organic solvent (acetonitrile and water; 15 ml, 60:40 v/v). They were sonicated (Fisher Scientific FS 20, Fairlawn, NJ, USA) for 4 h to remove PTX for HPLC analysis (Shimadzu SP-10A VP, Columbia, MD, USA). HPLC analysis for PTX was performed on a C18 Zorbax column (150 x 4.6 mm, 5 µm; Phenomenex, Torrance, CA, USA) with a mobile phase consisting of 0.1M methanol (v/v/v) at a flow rate of 0.75 ml/min. Effluents were monitored at 227 nm and measured using the area under the peak from standard solutions dissolved in mobile phase (0.4 to 2 µg/ml) [18].

In Vitro Studies

Mathematical model of drug loading efficiency and release kinetics of PTX

The loading content (LC) and encapsulation efficiency (EE) of PTX were analysed using high-performance liquid chromatography (HPLC, Shimadzu SP-10A VP, (250 × 4.6 mm) Columbia, MD, USA) consisting of a P-900 gradient pump system and an Ultra C18 5 µm column. 1 mg of PTX/GO/H-n-HAP was first dissolved in dichloromethane (DCM) for 30 min. The resulting solution was then passed through a 0.45 µm filter. HPLC analysis was performed at a flow rate of 1.0 mL/min at 37°C using acetonitrile/water (v/v = 4:1) as mobile phase and detected at a wavelength of 227 nm (UV detector, Shimadzu SP-10A VP). LC and EE were calculated according to the following equations:

$$LC\% = \frac{weight\ of\ loaded\ drug}{weight\ of\ drug\ loaded - NP_s} x\ 100\% \quad (1)$$

$$EE\% = \frac{weight\ of\ loaded\ drug}{weight\ of\ drug\ feed} x\ 100\% \quad (2)$$

Cytotoxicity and cell culture

In vitro cell culture studies were conducted using the AsPC-1 (ATCC® CRL-1682™) pancreatic cell line derived from a metastatic site, while normal pancreatic cells (CRL-4023 human pancreatic duct epithelium) were used as a control. The cells were cultured in IMDM culture medium supplemented with 10% FBS, maintained at 37°C under 5% CO2. Passaging was performed every 72 hours. After one week, the cells were digested with trypsin containing 2% EDTA and washed with PBS. The resulting supernatant was discarded, and the cells were counted. To create frozen stocks, the cells were frozen in liquid nitrogen and subsequently thawed at 37°C. This freeze-thaw process was repeated three times. For the cytotoxicity assay, AsPC-1 pancreatic cells were seeded in 96-well plates at a density of 10,000 cells per well. The plates were then incubated in a 37°C incubator with 5% CO2 for 24 hours. The synthesized nanostructure was tested at two different concentrations (0.01 mg/ml and 0.05 mg/ml) on the AsPC-1 pancreatic cell line. Three replicates of each concentration were used. The compounds of different concentrations were added to the wells and incubated for 48 hours in the same incubation conditions. To assess cell viability, the MTT (3-(4,5-dimethylthiazol-2-yl)-2,5-diphenyltetrazolium bromide) assay was performed. In this assay, 10 µl of MTT salt solution was added to each well and incubated for 3 hours at 37°C. After the formation of formazan crystals, 100 µl of dimethyl sulfoxide (DMSO) was added to each well and kept in the dark for 30 minutes. The absorbance was then measured at 570 nm using an ELISA reader. Tumor cell antigens were prepared by centrifuging the cells at 1000 rpm for 5 minutes, followed by filter sterilization [19], [20].

Result And Discussion

Particle Size, Size Distribution and Zeta Potential

Zeta potential is related to surface charge density and double layer thickness. The surface charge density depends on the concentration of potential-determining ions. Since H+ ion is the potential-determining ion in many systems, the zeta potential depends on pH. The zeta potential is positive for low pH values and negative for high pH values. As seen in the graph, the zeta potential values of all samples were negative. As a result, this showed that the prepared samples were successfully produced at the desired pH values. When hydrothermal method was applied to n-HAP and PTX was loaded to H-n-HAP and H-n-HAP/GO, zeta potential values were observed more. This showed that the stability of the hydrothermally treated samples increased, i.e. the degradation rates decreased. However, the stability of PTX-loaded H-n-HAP and PTX-loaded H-n-HAP/GO was found to be higher than that of H-n-HAP alone. This implies that when the designed drug system is administered intravenously to the patient, the residence time in the blood will be higher than PTX alone. In conclusion, in zeta potential analysis, the more charged a

sample is, the better it disperses. A low zeta potential of the sample indicates that the material tends to agglomerate. Agglomeration causes embolization and clogs the vessel. A high zeta potential indicates that the designed drug delivery system will not cause vascular occlusion.

Table 1. Physicochemical characterization (Particle size, zeta potential, conductivity, electrophoretic) of PTX loaded H-n-HAP and H-n-HAP

Samples	Particle size (nm)	Zeta potential (mV)	Conductivity [mS/cm]	Electrophoretic [cm^2/Vs]
H-n-HAP	815.12±8.35	-10.2±0.2	0.109	-30.10^{-6}±4. 10^{-6}
H-n-HAP/PTX(1mg)	446.17±3.66	-12.5±0.24	0.107	-49.10^{-6} ±3. 10^{-6}
H-n-HAP/PTX(2mg)	349.17±5.66	-16.1±0.24	0.112	-55.10^{-6}±3. 10^{-6}
H-n-HAP/GO%1	668.34±4.75	-29.5±0.12	0.152	-69.10^{-6}±5. 10^{-6}
H-n-HAP/GO%0.5	537.06±1.99	-27.2±0.43	0.132	-67.10^{-6}±5. 10^{-6}
H-n-HAP/GO%1-PTX(1mg)	226.7±0.70	-36.8±1.4	0.144	-76.10^{-6}±5. 10^{-6}
H-n-HAP/GO%0.5-PTX(2mg)	194.74±1.04	-35.6±1.2	0.133	-71.10^{-6}±5. 10^{-6}

BET analysis

Measurement of porous surface area and pore size by BET adsorption and desorption of Nitrogen (N_2) gas emission was performed. N_2 utilization based on adsorption by surface area can then be evaluated by N_2 gas consumed pore dispersion.

Table 2. BET and BJH adsorption & desorption (H-nHAP, H-n-HAP/GO, H-n-HAP/PTX, H-n-HAP/GO-PTX samples)

Samples		H-n-HAP	H-n-HAP/GO	H-n-HAP/PTX	H-n-HAP/GO-PTX
Spesific Surface Area (m^2/g)	BET	81.47	42.19	71.11	58.19
	Largmuir	187.12	82.85	172.85	152.85
	BJH Adsoption	80.93	38.20	71.20	63.34
	BJH Desorption	82.05	41.892	73.89	68.08

Table 2 shows the data obtained as a result of BET analysis. According to the results obtained, the specific surface area of PTX-loaded H-n-HAP was 71.11 m^2/g and the surface area of PTX/GO-loaded H-n-HAP was 58.19 m^2/g. GO loaded H-n-HAP surface area was 42.19 m^2/g. To see the difference in the surface area of the additives here, the H-n-HAP surface area was measured and found to be 81.47 m^2/g. As a result, it was observed that the more the H-n-HAP crystal structure is realized, the larger the surface area of the dopants.

FTIR Analysis

FTIR spectra magnification analysed between 4000 and 750 cm^{-1} wavenumbers (Figure 1). As a result of FTIR analysis of H-n-HAP functional groups; O-H bonds show a peak at 3378.51 cm^{-1}. A peak was observed at 1657.52 cm^{-1} for C=O bonds, 1051.07 cm^{-1} for P-O bond and 976.44 cm^{-1} for C=O. As a result of FTIR analysis of H-n-HAP functional groups, O-H bonds show a peak at 3388.93 cm-1. C=O bonds show a peak at 1421.54 cm^{-1}, P-O bond at 1020.34 cm^{-1} and C=O at 962.48 cm^{-1}.

As a result of FTIR analysis of PTX-loaded H-n-HAP functional groups; O-H bonds show a peak at 3425.58 cm^{-1} and a peak of C-H bond at 1338.60 cm^{-1}. A new peak appeared at 1658.78 cm^{-1} and was not found in PTX and pure hydroxyapatite. The new peak 1 at 1658.78 cm-1 may be due to PTX at 1543.05 cm^{-1} and undegraded HAP at 1427.32 cm^{-1}. A P-O peak is observed at 1028 cm^{-1}. The band at 1338 cm^{-1} does not exhibit a distinct shift, suggesting the absence of chemical bonding between HAP surface calcium ions and PTX radicals. The mechanism of drug loading appears to be mainly by electrostatic interaction between the positive calcium ions on the HA surface and the negative carboxylate radical on PTX.

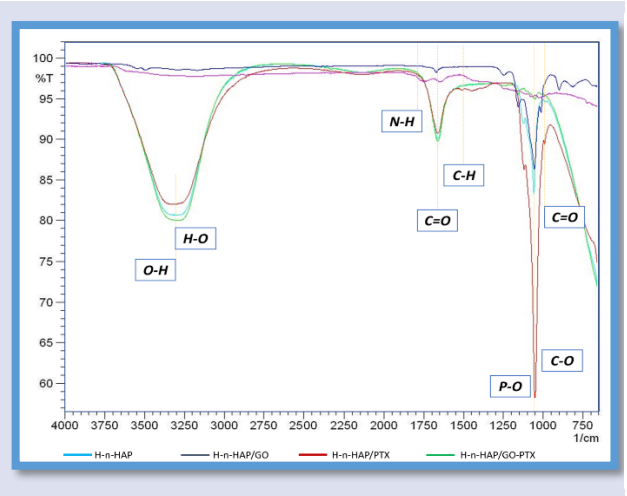

Figure 1. H-n-HAP, H-n-HAP/GO, H-n-HAP/PTX and H-n-HAP/GO-PTX of FTIR analysis

PTX-loaded H-n-HAP functional groups; a peak at 3394.72 cm^{-1} for O-H bonds and a peak at 1338.60 cm^{-1} for C-H bonds were observed. At 1651.07 cm^{-1}, new peaks without PTX and H-n-HAP appeared. The peak at 1651.07 cm^{-1} was observed to be due to the PTX at 1543.05 cm^{-1} and the undegraded H-n-HAP at 1421.54 cm^{-1}. At 1020.34 cm^{-1}, a peak belonging to P-O is observed. The band at

1338 cm^{-1} does not exhibit a distinct shift, suggesting the absence of chemical bonding between H-n-HAP surface calcium ions and PTX carboxylate radicals. The mechanism of drug loading was observed mainly by electrostatic interaction between the positive calcium ions on the HAP surface and the negative carboxylate radical on PTX. PTX functional groups O-H bonds by FTIR spectroscopy show a peak at 3388.93 cm^{-1}. A peak for N-H bond at 1543.05 cm^{-1}, a peak for C-H bond at 1338.60 cm^{-1} and a peak for C-O bond at 1031.92 cm^{-1} were observed.

XRD Analysis

When the XRD patterns of H-n-HAP, GO, PTX, H-n-HAP/GO, H-n-HAP/PTX and H-n-HAP/GO/PTX were compared, it was observed that the characteristic peaks of the crystal structures in H-n-HAP form and GO and PTX materials loaded into H-n-HAP crystal form were thinner and sharper (Figure 2).

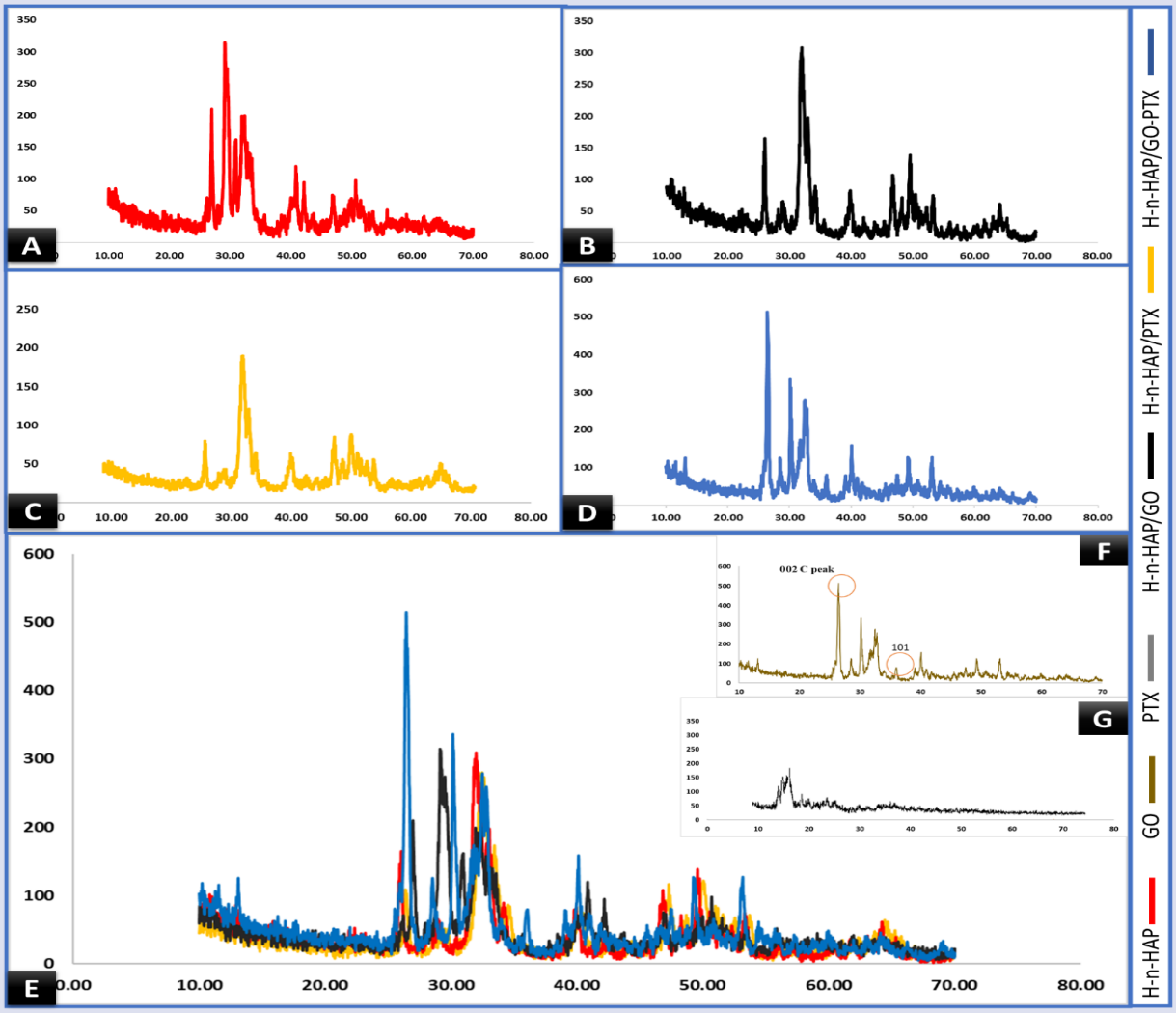

Figure 2. XRD of H-n-HAPs; A. H-n-HAP, B. H-n-HAP/GO, C. H-n-HAP/PTX, D. H-n-HAP/GO-PTX, E. All XRD pattern, F. GO, G. PTX

In a similar study, selective laser sintered H-n-HAP composite microspheres were designed for BTE applications. The XRD curves of nano-HA showed that the crystallization peaks of typical HAP, such as three strong peaks (211) (112) (300), correspond to angles of 31.93°, 32.65° and 33.82°, respectively [21]. These and similar studies support our XRD analysis as shown in Figure 2. For the XRD of amorphous materials, the position of the peak corresponded to the average distance between the chains [22]. The larger the average interchain distance, the smaller the angle. Thus, the value of the composites increased due to the introduction of H-n-HAP, while the non-crystalline peak of the composites shifted slightly to the left. Moreover, the presence of at least two peaks indicated that the materials have multiple average interchain distances [23].

TGA Analysis

The decomposition behaviour was studied by DTA and TGA curves for H-n-HAP/PTX and H-n-HAP/GO/PTX nanocomposite powders, Figure 3. The curves are divided into two endothermic zones ranging from 25 to 200 °C, the peak existing at about 250 °C corresponding to a 6% moisture loss due to thermal stability in H-n-HAPs. When

the temperature range was increased by 200-1000 °C, it corresponded to the de-hydroxylation precipitation complex due to OH loss and the loss of physically adsorbed water molecules of the H-n-HAP powder. This is shown in Region II.

In the TG-DTA plot of PTX-loaded H-n-HAP, a 14% loss of n-HAPs was observed. The loss in H-n-HAPs was observed to be about 6%. When H-n-HAP was compared with PTX-loaded H-n-HAP, it was observed that the loss of approximately 8% could be due to PTX in the drug system, lactose monohydrate and methylparaben.

For TG-DTA of PTX-loaded H-n-HAP/GO, a 4% loss in n-HAPs was observed. Compared to PTX-loaded H-n-HAP, the loss is less here. This may be because the drug PTX is incorporated into the n-HAP crystal, so it is not lost during the process or some molecules in the drug are disrupted during the hydrothermal process.

The thermal stability of H-n-HAP/PTX containing 1% GO at a temperature of about 200°C, where the thermal stability of GO decreased due to carboxylic decomposition and release of CO_2 gas and 1% of GO mass was lost [36].

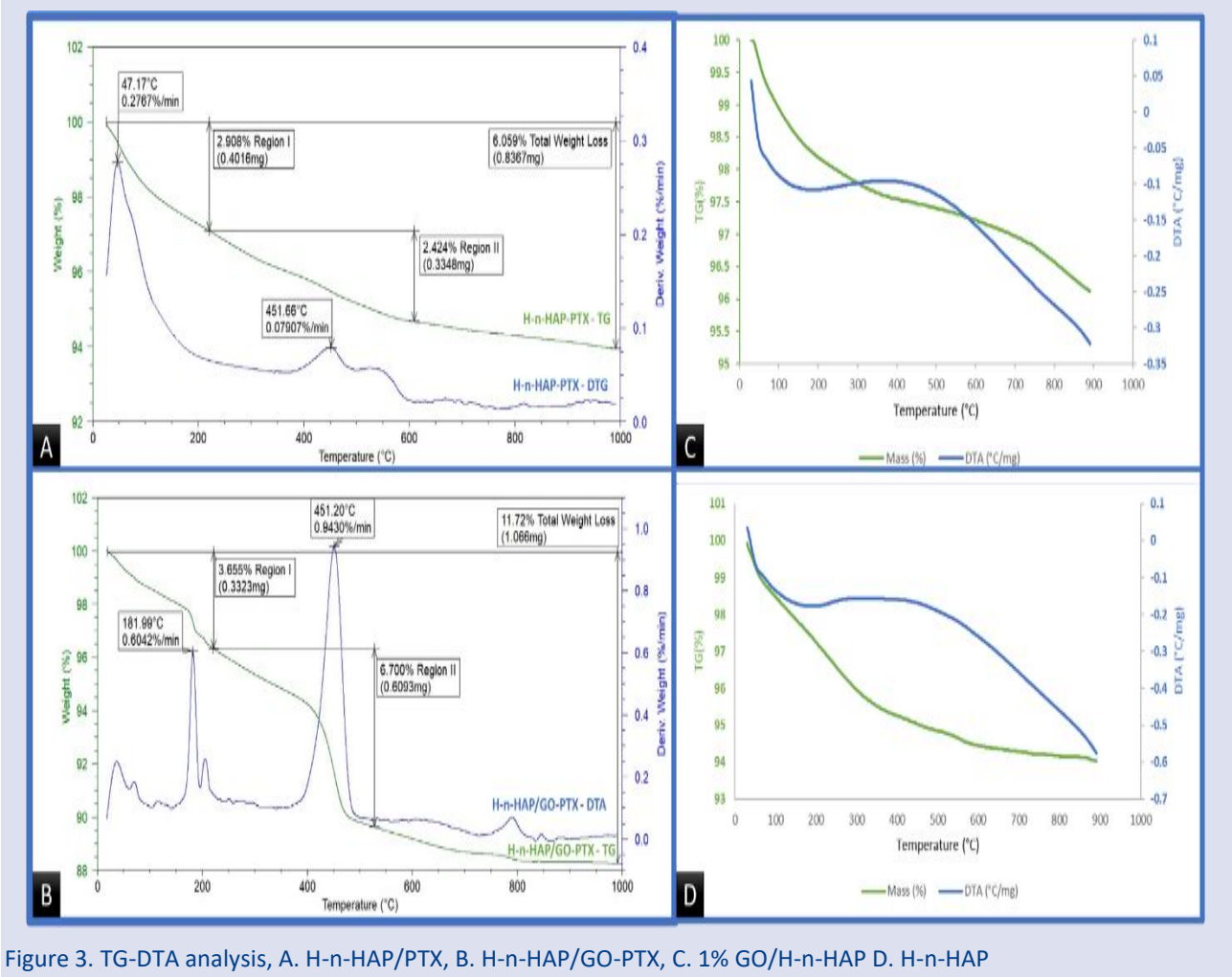

Figure 3. TG-DTA analysis, A. H-n-HAP/PTX, B. H-n-HAP/GO-PTX, C. 1% GO/H-n-HAP D. H-n-HAP

SEM and EDS Mapping / Spotting

In the SEM image for H-n-HAP/GO-PTX in Figure 4.D, a zoom of 2 µm was made, two different sizes were measured with ImageJ program in two different regions and seen as 153 nm and 438 nm, respectively. For H-n-HAP/GO, Figure 4.B shows the presence of GO nanostructures. It was observed that GO doped into H-n-HAP production enhanced the crystal surface growth of n-HAP. Even 1% doping of GO was observed to increase porosity with high surface area. The homogeneous distribution of n-HAPs synthesized by hydrothermal method showed the suitability of the studies carried out at the point of PTX doping [6], [24].

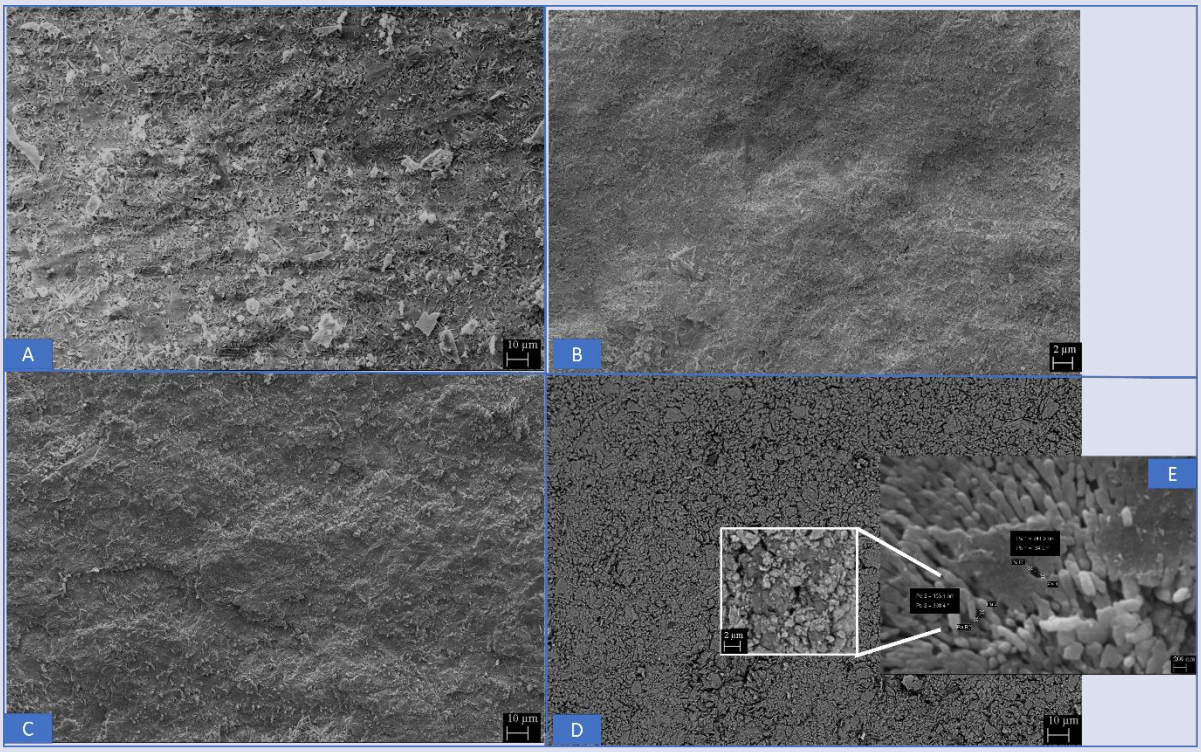

Figure 4. SEM of H-n-HAPs, size measurement at 200nm for A. H-n-HAP, B. H-n-HAP/GO, C. H-n-HAP/PTX, D. H-n-HAP/GO-PTX, E. H-n-HAP/GO-PTX; ImageJ

By EDS spotting, 3 different regions of the H-n-HAP/GO-PTX therapeutic nanoparticle structure were selected and the homogeneous distribution of the nanocomposite structure was confirmed (Figure 5).

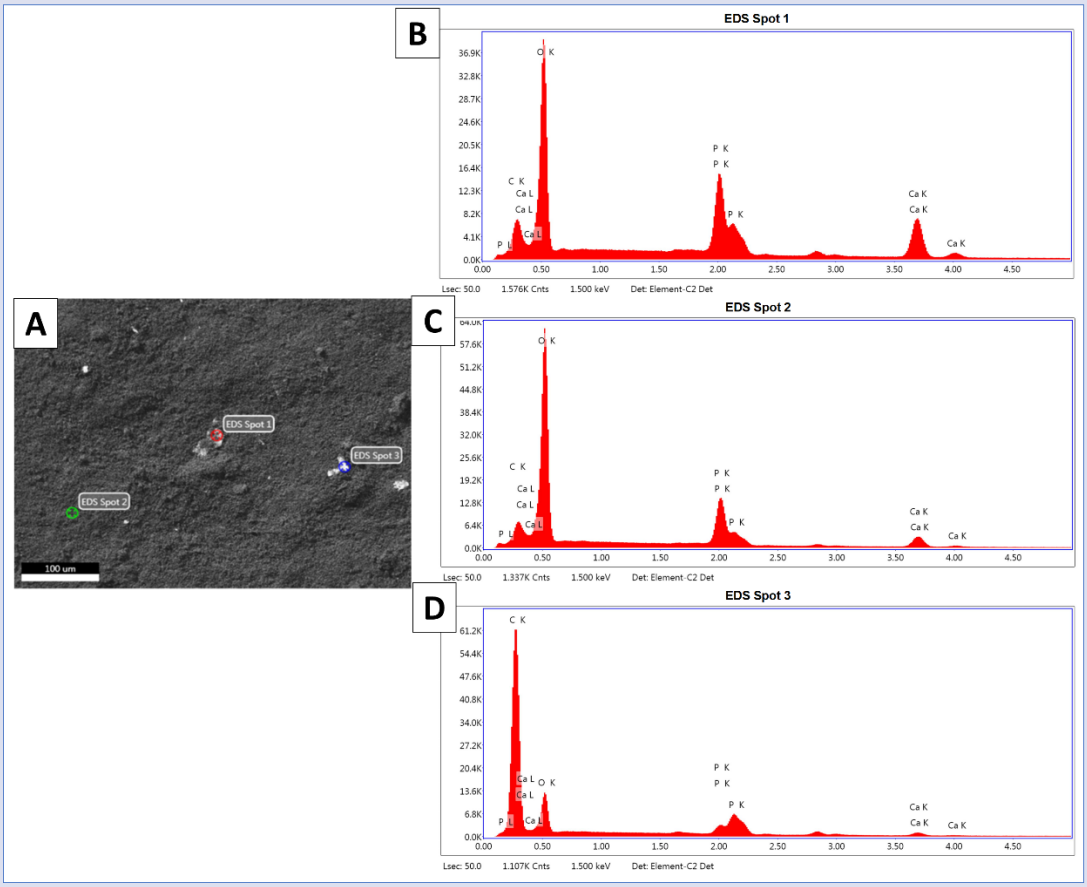

Figure 5. A. EDS mapping analysis and element analysis of nanoparticles samples. Three chosen spot to compare elementally in B. Spot 1, C. Spot 2, D. Spot 3

In EDS spot 1, EDS spot 2 and EDS spot 3 observations, the Ca/P ratio was approximately 1.66 and the elemental values were close to each other between the sintered and unsintered samples. The Ca/P ratio of the synthesized nanocomposite materials was found to be 1.69 ± 0.053. In the literature, n-HAP Ca/P ratio, which is considered thermodynamically stable, is known as 1.67. The difference in this study was estimated that the GO structure and PTX pharmodynamic effect may have increased the surface area. However, this will not change our conclusion that the result is close to the literature information, on the contrary, it will confirm it [25], [26].

Chromatographic Performance of PTX

The linearity of the method used for PTX was evaluated on the calibration curve of the assay. In Figure 6 the components of the drug PTX are shown in the peak areas. The specificity/selectivity of the analytical method was confirmed by analysing solutions containing 100% of the normal working concentration. The compositions of PTX, the pharmaceutical product tested qualitatively and quantitatively were determined by this analysis. The solubility between the peaks corresponding to the various substances of the pharmaceutical drug present in the GO and PTX formulations doped with H-n-HAPs, especially for the compounds with the closest elution concerning PTX, was analysed and shown in Figure 6.A with figures. According to these results; Figure 6.A1; 10-deacetyl-paclitaxel, Figure 6.A2; 10-deacetyl-7-epi-paclitaxel, Figure 6.A3; paclitaxel, Figure 6.A4; 7-epi-paclitaxel, Figure 6.A5; 10-deacetyl-bacatin III. A comparative analysis of the chromatograms (plate number, flow rate, and bar; Table 3) is shown in Figure 6.B. If the impurities eluted after PTX were > 1 with relative retention time (RRT), they were masked by the excipient matrix. Due to this interference, the method is not recommended for purity control in finished products. PTXs were preserved by doping into hydrothermally produced n-HAPs.

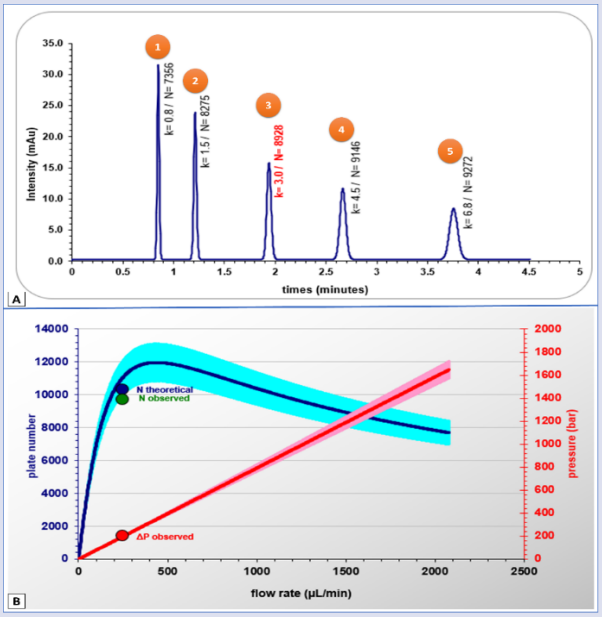

Figure 6. Chromatographic performance in isocratic mode, A. Chromatographic conditions, B. chromatographic performance

Table 3. HPLC method for PTX drug conditions and performance

Chromatographic conditions		Chromatographic performance	
Stationary support	Zorbax extend	Optimal flow rate	434 ul/min
Length	50 mm	Suggested working flow rate	887 ul/min
Diameter	2.1 mm	N theoretical	10319
Particle size	1.7 um	N observerd (for UPLC only)	9683
Organic solvent	(MeOH)	%N loss (due to UPLC instrumentation)	6%
Mobile phase temperature	65 °C	%N loss (due ton on-optimal flow rate)	%14
Mobile phase composition (%organic)	40%	%N loss (total)	%20
Flow-rate	250 ul/min	ΔP observed	198 bar
Solute molecular mass	200 g/mol		
Injection volüme	2.0 uL		
Detector time constant	100 ms		
Average retention factor –(k)	3		

PTX Loading Efficiency, Release Kinetics Mathematical Model

Polydispersity Index (PDI), Drug Loading Content (LC) and Encapsulation Efficiency (EE) values of PTX-loaded H-n-HAP and H-n-HAP/GO nanocrystalline composites at different mass ratios was showed in Table 4. When PTX was 1 and 2 mg, EE and LC were 79.17-72.24% and 80.01-80.27%, respectively, for H-n-HAP crystal structure only, while EE and LC were 88.57-81.57% and 90.84-110.57%, respectively, when H-n-HAP crystal structure was loaded with 1 and 2 mg PTX together with GO. As expected, increases in LC were observed with GO doping in the loading.

Table 4. PDI, LC and EE of PTX-doped H-n-HAP and H-n-HAP/GO at different mass ratios of drug and carriers

Samples	PDI	EE (%)	LC (%)
H-n-HAP/PTX(1mg)	0.289±0.034	79.17±3.04	80.01±0.21
H-n-HAP/PTX(2mg)	0.295±0.024	72.24±1.18	80.27±0.67
H-n-HAP/GO%1-PTX(1mg)	0.369±0.045	88.57±2.53	90.84±1.47
H-n-HAP/GO%0.5-PTX(2mg)	0.410±0.034	81.57±2.04	110.57±0.81

Table 5. Mathematical kinetic release model parameters for in vitro release of paclitaxel from formulation H-n-HAP/PTX and H-n-HAP/GO-PTX

PTX Loaded samples	Time (hours)	Cumulative PTX release %	% Remaining PTX bioactive ingredient	Square root of time	log % remaining PTX bioactive substance	Time log	log Cumulative PTX release %	(Wt)	Wo-Wt
H-n-HAP	1-2	28.7-42.7	71.3-57.3	1.000-1.414	1.853-1.758	0.000-0.301	0.000-1.630	4.147-3.855	0.000-0.787
	4-6	58.7-67.9	41.3-32.1	2.000-2.449	1.616-1.507	0.602-0.778	1.769-1.832	3.457-3.178	1.185-1.464
	8-24	88.8-92.7	11.2-7.3	2.828-4.899	1.049-0.863	0.903-1.380	1.948-1.967	2.237-1.940	2.405-2.702
H-n-HAP/GO	1-2	33.3-48.9	66.7-51.1	1.000-1.414	1.824-1.708	0.000-0.301	0.000-1.689	4.055-3.711	0.000-0.931
	4-6	64.2-71.3	35.8-28.7	2.000-2.449	1.554-1.458	0.602-0.778	1.808-1.853	3.296-3.062	1.346-1.580
	8-24	88.9-99.5	11.1-0.5	2.828-4.899	1.045-(-0.301)	0.903-1.380	1.949-1.998	2.231-0.794	2.411-3.848

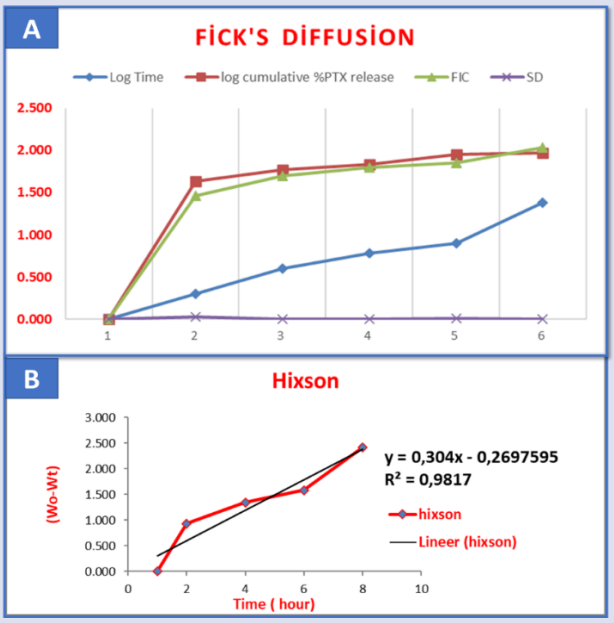

Figure 7. A. In vitro PTX release in Fick's diffusion law, B. Graphical representation of Hixson release model

During the preparation of PTX-loaded nanostructured composites from the co-delivery system PTX, GO carbon nanomaterials were chemically bound to the H-n-HAP structures and PTX molecules were physically loaded into the micelle core. The release profiles were pH-dependent, but the release mechanism needed to be studied. Here, the drug release mechanism was investigated using a comprehensive semi-empirical model. Based on the experimental data in Table 5, the drug release process was evaluated from 1-24 hours. The formulations used in this evaluation process were divided into two groups, H-n-HAP/PTX and H-n-HAP/GO/PTX. The results obtained according to the mathematical models of release kinetics in Table 5 are presented in a theoretical curve based on Fick's law (Figure 7.A). Here, it was observed that the release exponent (n) and rate constant (k) were by the Hixson model for the two stages of PTX release profiles (Figure 7.B). According to Fick's law, K=1.89, n=0.21, SSD=0.04, R^2=0.997, FIC=2.03, SD=0.004.

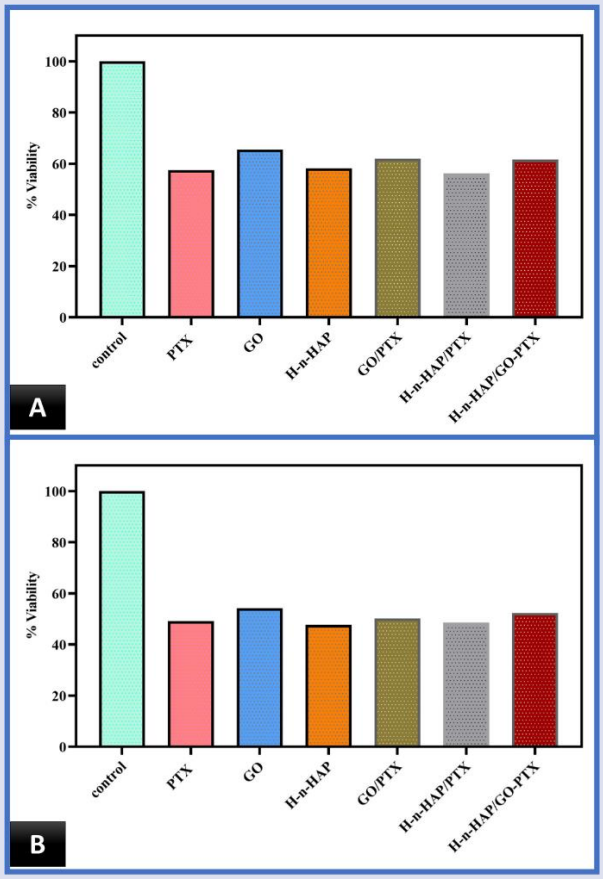

Figure 8. Graph for cell viability rate A. 10% concentration and B. 50% concentration

Cell Culture Study

In this graph, Figure 8.A shows the results of the MTT viability test for samples prepared at 10% concentration, while Figure 8.B shows the results of the MTT viability test for samples prepared at 50% concentration. At 10% concentration, the viability rate for H-n-HAP was 57.8%, for H-n-HAP/GO/PTX 59.8%, PTX 46.6%, H-n-HAP/GO 57.2% and PTX 48.8%. At 50% concentration, H-n-HAP viability was 40.5%, H-n-HAP/GO/PTX 49.5%, H-n-HAP/GO/PTX 38.8%, GO 43.4% and PTX 40.0%. As can be seen from the results, all samples were successful in

excluding cells in the pancreatic cancer cell line. As GO nanomaterials were loaded into the H-n-HAP nanocrystal structure, the effect of PTX drug on pancreatic cancer increased and the viability of cancer cells decreased. It can be concluded that H-n-HAP/GO/PTX nanocomposite structure kills more pancreatic cancer cells by synergetic effect [27], [28].

Simulation; In Silico Modelling

In the study, the absorption rate and duration of the 500 mg dose and its safety were modelled. This modelling for the bioavailability of PTX is a unique contribution to the literature. The low bioavailability of PTX is a factor that may reduce PTX efficacy. Although in vitro studies show the high efficacy of PTX in its biologically beneficial effects in cells, its distribution in tissues is known to be very low. Consequently, in vitro studies should be interpreted with caution when trying to predict their effect in vivo studies.

Due to its chemical and physical properties, PTX can passively cross cell membranes or interact with membrane receptors. It can therefore interact with extracellular and intracellular molecules. Its mechanism of action at the cellular level can therefore be triggered either by activating signalling pathways when binding to cell membrane receptors, by activating intracellular mechanisms, or even by developing its effects within the nucleus.

Controlled drug delivery devices have been envisioned in the reverse engineering framework for the controlled release of PTX, an anticancer drug widely used in the treatment of pancreatic cancer. A framework was established using quantitative structure-property relationship (QSPR) models for the mutual diffusion coefficients of PTX doped into the H-n-HAP/GO nanostructure we obtained as a biocompatible and biodegradable composite structure and the partition coefficients of the drug between polymers and blood. It was developed to predict optimal drug delivery devices for desired dosage regimens. In Franz diffusion modelling, release kinetics were based on Hixson. Based on the selected clinical application of pancreatic cancer, the optimal design parameters were estimated for the maximum bioavailability of the drug, along with the selection of the optimal polymeric composite H-n-HAP/GO suitable for different dosing regimens [29]–[31].

An *in-silico* fluid flow model with *in silico* assumptions (Figure 9.A and B) was used in Python program. In the reversible engineering problem, the objective was to maximize the bioavailability of the drug calculated in terms of AUC, while adjusting the drug concentration to ensure that the specified dosing regimens (24 h) remain within the therapeutic range. Genetic Algorithms (GA) implemented in Python were used to calculate Cmax, Tmax, and AUC. Python was used to simulate the drug release model (forward problem) while GA was used to solve the inverse problem. In GA, body weight was set to 70 and dose to 500 [32].

Table 6. *In vivo* Cp prediction from in vitro dissolution (AUC; area under the drug concentration and time curve)

Time	*1*	*2.00*	*4.00*	*6*	*8.00*	*24*	*Total amount after absorption*	*Con. (ng/ml) at a Time*	*[AUC $_{0-t}$]*
%PTX release	0	54	63	140	71.5	58.5			
	1	0					0	0.00	129.1454
	2.00	54					54	258.29	624.2379
	4.00	13.50735	63				76.51	365.95	1127.127
	6	3.378674	15.75857	140			159.14	761.18	1293.574
	8.00	0.845128	3.941787	35.01905	71.5		111.31	532.39	6497.742
	24.00	1.3E-05	6.04E-05	0.000537	0.001096	58.5	58.50	279.82	-3357.88

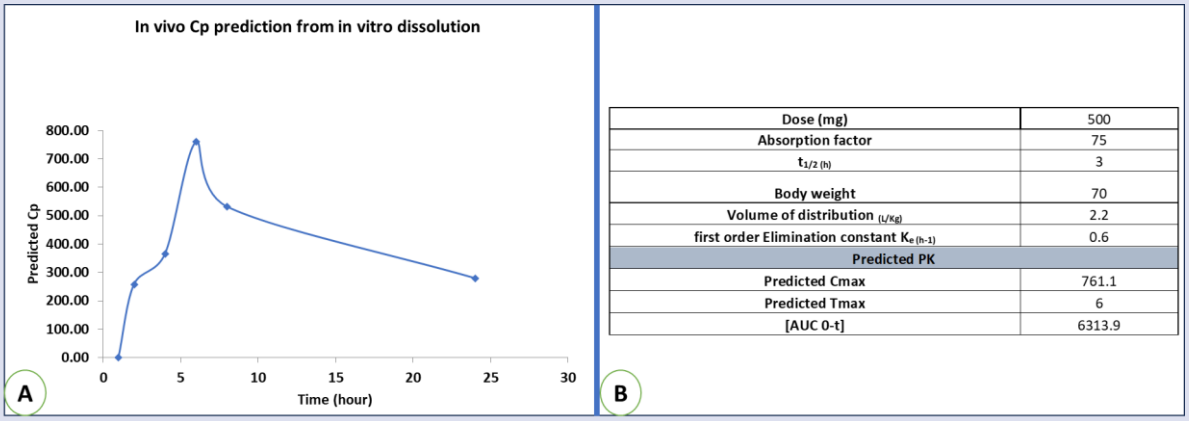

Figure 9. A. In vivo Cp prediction from in vitro dissolution, B. (Cmax; drug concentration in blood (mol/m3), Tmax; time at which the drug is desired to be released in the therapeutic range

Conclusion

The present study reverses engineered diffusion-controlled drug delivery devices of PTX, a drug used effectively in pancreatic cancer, by doping hydrothermally synthesized n-HAP crystals with GO, a surface activating carbon nanomaterial. The feasibility of the proposed approach was established using diffusion-controlled release of PTX, an established anti-cancer drug for the treatment of solid cancer. The synthesis of n-HAPs by hydrothermal method provides a large surface area, while GO-doped drug release kinetics are found to be enhanced. Mathematical models should be developed to design drug delivery systems in cancer types such as pancreatic cancer and should be actively used in in vivo and in vitro studies.

Conflicts of interest

The authors stated that did not have conflict of interests.

References

[1] V. Andretto, A. Rosso, S. Briançon, and G. Lollo, Nanocomposite systems for precise oral delivery of drugs and biologics, *Drug Deliv Transl Res.*, 11(2) 2021 445–470.

[2] F. Ciftci, Release kinetics modelling and in vivo-vitro, shelf-life study of resveratrol added composite transdermal scaffolds, *Int J Biol Macromol*., 235 (2023) 123769.

[3] S. Javanbakht and H. Namazi, Doxorubicin loaded carboxymethyl cellulose/graphene quantum dot nanocomposite hydrogel films as a potential anticancer drug delivery system, *Mater Sci Eng C.*, 87 (2018) 50–59.

[4] M. J. Mitchell, M. M. Billingsley, R. M. Haley, M. E. Wechsler, N. A. Peppas, and R. Langer, Engineering precision nanoparticles for drug delivery, *Nature Reviews Drug Discovery.*, 20(2) (2021) 101–124.

[5] Venkata V.V., Omathanu P.P., Nanosystems for Dermal and Transdermal Drug Delivery, in *Drug Delivery Nanoparticles Formulation and Characterization.*, 1st Edition. CRC Press, (2020) 146–175.

[6] A. C. Özarslan, C. Özel, M. D. Okumuş, D. Doğan, and S. Yücel, Development, structural and rheological characterization, and in vitro evaluation of the zinc-doped 45S5 bioactive glass-vaseline ointment for potential wound healing applications, *J Mater Res*, (2023).

[7] S. Hussain and K. Sabiruddin, Synthesis of eggshell based hydroxyapatite using hydrothermal method, *IOP Conf Ser Mater Sci Eng.*, 1189(1) (2021).

[8] H. S. Liu *et al.*, Hydroxyapatite synthesized by a simplified hydrothermal method, *Ceram Int.*, 23(1) (1997) 19–25.

[9] Y. P. Guo, Y. B. Yao, C. Q. Ning, Y. J. Guo, and L. F. Chu, Fabrication of mesoporous carbonated hydroxyapatite microspheres by hydrothermal method, *Mater Lett.*, 65(14) (2011) 2205–2208.

[10] G. Zhang, J. Chen, S. Yang, Q. Yu, Z. Wang, and Q. Zhang, Preparation of amino-acid-regulated hydroxyapatite particles by hydrothermal method, *Mater Lett.*, 65(3) (2011) 572–574.

[11] A. Razaq, F. Bibi, X. Zheng, R. Papadakis, S. H. M. Jafri, and H. Li, Review on Graphene-, Graphene Oxide-, Reduced Graphene Oxide-Based Flexible Composites: From Fabrication to Applications, *Materials*, (2022).

[12] A. Jiříčková, O. Jankovský, Z. Sofer, and D. Sedmidubský, Synthesis and Applications of Graphene Oxide, *Materials*., (2022).

[13] A. Raslan, L. Saenz del Burgo, J. Ciriza, and J. Luis Pedraz, Graphene oxide and reduced graphene oxide-based scaffolds in regenerative medicine, *Int J Pharm*, 580 (2020) 119226.

[14] C. Daulbayev *et al.*, Effect of graphene oxide/hydroxyapatite nanocomposite on osteogenic differentiation and antimicrobial activity, *Surfaces and Interfaces.*, (2022).

[15] F. Ciftci *et al.*, Selenium and clarithromycin loaded PLA-GO composite wound dressings by electrospinning method, *Int J Polym Mater Polym Biomater.*, (2022).

[16] M. S. Al Mogbel, M. T. Elabbasy, M. F. H. Abd El-Kader, R. S. Mohamed, M. E. Moustapha, and A. A. Menazea, Morphological, mechanical, and antibacterial investigation of a ternary nanocomposite contains hydroxyapatite, tellurium(IV) oxide (Te2O4), and graphene oxide in vitro, *Appl Phys A Mater Sci Process.*, (2022).

[17] Z. Benzait, P. Chen, and L. Trabzon, Enhanced synthesis method of graphene oxide, *Nanoscale Adv.*, (2021).

[18] F. Ciftci *et al.*, Antibacterial and cellular behavior of PLA-based bacitracin and zataria multiflora nanofibers produced by electrospinning method, *Int J Polym Mater Polym Biomater*, 72(4) (2023) 319–334.

[19] B. Wójcik *et al.*, Effects of metallic and carbon-based nanomaterials on human pancreatic cancer cell lines aspc-1 and bxpc-3, *Int J Mol Sci.*, 22(2) (2021).

[20] S. S. Kim *et al.*, Hyperthermal paclitaxel-bound albumin nanoparticles co-loaded with indocyanine green and hyaluronidase for treating pancreatic cancers, *Arch Pharm Res.*, 44(2) (2021) 182–193.

[21] K. Lin *et al.*, Selective laser sintered nano-HA/PDLLA composite microspheres for bone scaffolds applications, *Rapid Prototyp J.*, (2020).

[22] Y. Chen *et al.*, Dual Template, Three-Dimensional Hierarchical Porous Scaffolds Based on Graphene Oxide for Bone Tissue Engineering, *ECS Meet Abstr.*, (2020).

[23] J. Prakash, D. Prema, K. S. Venkataprasanna, K. Balagangadharan, N. Selvamurugan, and G. D. Venkatasubbu, Nanocomposite chitosan film containing graphene oxide/hydroxyapatite/gold for bone tissue engineering, *Int J Biol Macromol.*, (2020).

[24] A. C. Özarslan and S. Yücel, Comprehensive assessment of SrO and CuO co-incorporated 50S6P amorphous silicate bioactive glasses in vitro: Revealing bioactivity properties of bone graft biomaterial for bone tissue engineering applications, *Ceram Int.*, (2023).

[25] I. P. Khosalim, Y. Y. Zhang, C. K. Y. Yiu, and H. M. Wong, Synthesis of a graphene oxide/agarose/hydroxyapatite biomaterial with the evaluation of antibacterial activity and initial cell attachment, *Sci Rep.*, (2022).

[26] F. Miculescu *et al.*, Considerations and Influencing Parameters in EDS Microanalysis of Biogenic Hydroxyapatite, *J Funct Biomater.*, (2020).

[27] A. C. Özarslan, Y. B. Elalmis, and S. Yücel, Production of biosilica based bioactive glass-alginate composite putty as bone support material, and evaluation of in vitro properties; bioactivity and cytotoxicity behavior, *J Non Cryst Solids*, (2021).

[28] M. N. Ozder, F. Ciftci, O. Rencuzogullari, E. D. Arisan, and C. B. Ustündag, In situ synthesis and cell line studies of nano-hydroxyapatite/graphene oxide composite materials for bone support applications, *Ceram Int.*, (2023).

[29] M. Ikram *et al.*, Photocatalytic and antibacterial activity of graphene oxide/cellulose-doped TiO2 quantum dots: in silico molecular docking studies, *Nanoscale Adv.*, 4(18) (2022) 3764–3776.

[30] A. Alangari *et al.*, Antimicrobial, anticancer, and biofilm inhibition studies of highly reduced graphene oxide (HRG): In vitro and in silico analysis, *Front Bioeng Biotechnol.*, 11 (2023).

[31] E. Peng, N. Todorova, and I. Yarovsky, Effects of Size and Functionalization on the Structure and Properties of Graphene Oxide Nanoflakes: An in Silico Investigation, *ACS Omega.*, 3(9) (2018) 11497–11503.

[32] P. S. Gade, R. M. Sonkar, and P. Bhatt, Graphene oxide-mediated fluorescence turn-on GO-FAM-FRET aptasensor for detection of sterigmatocystin, *Anal Methods.*, 14(39) (2022) 3890–3897.